

RECORDS ADMINISTRATION



AGTM

ACC # 735049

SRL

RECORD COPY

DP-MS-78-63

A HIGH-ORDER ACCURATE NUMERICAL ALGORITHM FOR
THREE-DIMENSIONAL TRANSPORT PREDICTION

by

D. W. Pepper and A. J. Baker

Proposed for Publication in *Computers and Fluids*

This paper was prepared in connection with work under Contract No. AT(07-2)-1 with the U. S. Department of Energy. By acceptance of this paper, the publisher and/or recipient acknowledges the U. S. Government's right to retain a nonexclusive, royalty-free license in and to any copyright covering this paper, along with the right to reproduce and to authorize others to reproduce all or part of the copyrighted paper.

This document was prepared in conjunction with work accomplished under Contract No. DE-AC09-76SR00001 with the U.S. Department of Energy.

DISCLAIMER

This report was prepared as an account of work sponsored by an agency of the United States Government. Neither the United States Government nor any agency thereof, nor any of their employees, makes any warranty, express or implied, or assumes any legal liability or responsibility for the accuracy, completeness, or usefulness of any information, apparatus, product or process disclosed, or represents that its use would not infringe privately owned rights. Reference herein to any specific commercial product, process or service by trade name, trademark, manufacturer, or otherwise does not necessarily constitute or imply its endorsement, recommendation, or favoring by the United States Government or any agency thereof. The views and opinions of authors expressed herein do not necessarily state or reflect those of the United States Government or any agency thereof.

This report has been reproduced directly from the best available copy.

Available for sale to the public, in paper, from: U.S. Department of Commerce, National Technical Information Service, 5285 Port Royal Road, Springfield, VA 22161, phone: (800) 553-6847, fax: (703) 605-6900, email: orders@ntis.fedworld.gov online ordering: <http://www.ntis.gov/ordering.htm>

Available electronically at <http://www.doe.gov/bridge>

Available for a processing fee to U.S. Department of Energy and its contractors, in paper, from: U.S. Department of Energy, Office of Scientific and Technical Information, P.O. Box 62, Oak Ridge, TN 37831-0062, phone: (865) 576-8401, fax: (865) 576-5728, email: reports@adonis.osti.gov

A HIGH-ORDER ACCURATE NUMERICAL ALGORITHM FOR THREE-DIMENSIONAL TRANSPORT PREDICTION

D. W. Pepper
Savannah River Laboratory
Aiken, S. C. 29801

A. J. Baker
Associate Professor
University of Tennessee

Abstract

The numerical solution of three-dimensional pollutant transport is calculated by the method of second moments for advection and the method of cubic splines for diffusion. The governing equation is solved by the technique of fractional steps. Topography and variable mesh spacing are accounted for with coordinate transformations. First estimate wind fields are obtained by interpolation to grid points surrounding specific data locations. Mass consistency is ensured by readjusting the three dimensional wind field with a Sasaki variational technique. Numerical results agree with predictions using conventional Gaussian plume relations for ideal conditions. The numerical model is used to predict three-dimensional transport of a release of tritium from the Savannah River Plant on May 2, 1974. Predicted ground level air concentration at 56km from the release point is within 38% of the experimentally measured value.

INTRODUCTION

The transport of radioactive and nonradioactive pollutants released from a source requires accurate predictions in order to assess potential hazards to the public. Environmental modeling of such releases is necessary not only for atmospheric problems, but also for problems dealing with estuary, river, stream, and ground water flows.

Under ideal conditions, the dispersion of pollutant concentration from a source can be calculated by analytical methods. However, analytical methods are not flexible enough to handle complex cases of three-dimensional, time-dependent dispersion where numerous parameters are constantly changing. Numerical models, while more flexible in solving complex transport problems, suffer from numerical dispersion errors.

In an effort to minimize numerical errors, a three-dimensional second-moments method calculates pollutant advection. This method is based on the calculation of moment distributions of a concentration within a cell (Egan and Mahoney, [1]; Pedersen and Prahm [2]; Fischer, [3]; Pepper and Long, [4]). By summing the moments over the entire solution domain, and using a Lagrangian advection scheme, a concentration field can be transported without numerical dispersion errors. Because the method maintains subgrid-scale resolution, point and area source releases can be calculated without significant

computational damping. To reduce computer programming complexity and computation time, the technique of fractional steps (Yanenko [5]) is used to solve the three-dimensional advection equation.

Three dimensional diffusion is solved by the method of cubic splines (Price and MacPherson, [6]; Rubin and Graves [7]; Ahlberg, et al., [8]; Fyfe, [9]). The cubic spline method is based on continuous-curvature cubic spline relations used as interpolation functions for first and second derivative terms. This method was preferred to other methods because of its unique characteristics: 1) the governing matrix system is always tri-diagonal; 2) second order derivatives are second order accurate even with large irregularities in mesh spacing; and 3) derivative boundary conditions can be applied with less difficulty than with conventional finite difference schemes. First order derivatives are fourth order accurate for uniform mesh and third order accurate for non-uniform mesh. After solution of the diffusion terms, the first and second moments are recalculated to ensure continuity with the advection terms.

Atmospheric concentrations are estimated to a distance of 100 km from the source with the three-dimensional second-moment/cubic spline technique. Mesoscale analysis of winds, temperatures, and eddy diffusivities are obtained from a network of towers situated throughout the 770 square kilometers of the

Savannah River Plant site near Aiken, South Carolina. The wind data are continuously updated, and the three-dimensional wind field is interpolated at all grid points. In order to make the wind field mass consistent, a Sasaki variational analysis (Lagrangian multipliers) is used to adjust the velocity components throughout the solution domain. The Lagrangian multipliers are calculated by the three-dimensional strongly implicit procedure (SIP).

Ground level predictions for tritium are compared with the experimental data obtained after the accidental release of tritium on May 2, 1974 from SRP. The effect of topography on plume emissions is also examined under ideal conditions. Numerical results are compared with values from the conventional Gaussian plume relations.

Mathematical Model

The governing equation for three-dimensional, time-dependent pollutant transport can be written as

$$\frac{\partial C}{\partial t} + \vec{U} \cdot \nabla C = \nabla \cdot (\hat{K} \nabla C) + S \quad (1)$$

where C is the concentration (gm/m^3), \vec{U} is the vector velocity field (m/sec), \hat{K} is the directionally dependent eddy diffusivity (exchange coefficient of diffusion, m^2/sec), and S represents the source and sink terms associated with precipitation scavenging, source emission, deposition, and chemical reaction.

The partial differential equation

established by Equation 1 is solved within the physical region, $x_W < x < x_E$, $y_S < y < y_N$, $h(x,y) < z < H$ for $t > 0$, where x_W , x_E , y_S , y_N are the west, east, south, and north lateral boundaries within the x-y plane, $h(x,y)$ is the ground elevation at (x,y) , and H is the elevation of the upper limit for vertical mixing (lid). An analogous equation which includes a variable mixing height, $H(x,y,t)$, is used by Reynolds, et al. [10]. Because this study is concerned with releases which occur over only a few hours, the variation of the mixing height is assumed to be negligible.

The initial condition on Equation 1 is that the mean concentration (C_0) is everywhere 0

$$C_0(x,y,z,t) = 0 \quad (2)$$

The mean concentration can also be specified at all locations as some initial background value. The following set of boundary conditions constrain the solution to the domain of interest:

$$\begin{aligned} \text{for } z = h(x,y), \\ -\hat{k}\nabla C_0 \cdot \hat{n}_h = f_0 \end{aligned} \quad (3)$$

$$\begin{aligned} \text{for } z = H, \\ -\hat{k}\nabla C_0 \cdot \hat{n}_H = 0 \end{aligned} \quad (4)$$

$$\begin{aligned} \text{for } x = x_W, x_E \text{ and } y = y_N, y_S \\ \vec{U} \cdot \hat{n} > 0, \quad -\hat{k} \cdot \nabla C_0 \cdot \hat{n} = 0 \end{aligned} \quad (5)$$

$$\vec{U} \cdot \hat{n} < 0, \quad (\vec{U} C_0 - \hat{k} \nabla C_0) \cdot \hat{n} = \vec{U} C_0 \cdot \hat{n} \quad (6)$$

where f_0 is the mass flux of concentration at the surface (for puffs or plumes, $f_0 \equiv 0$), \hat{n}_h is the unit vector normal to the surface while \hat{n}_H is the outwardly directed unit vector normal to the surface defined by the inversion base. The outwardly directed unit vector normal to the horizontal boundary is \hat{n} , and C_0' is the mean concentration just outside the solution domain.

The first condition specifies the diffusive component of the mass flux to be equal to zero when flow is out of the domain. The second condition requires continuity of mass flux across a boundary when flow is entering the solution domain. The lack of well posed boundary conditions does not cause serious problems since the advection terms in Equation 1 generally dominate the diffusive terms.

To account for deposition velocities at the surface, the flux at the ground can be expressed in terms of a deposition velocity (Calder, [11]) such that

$$pC \approx v_g C + K_z \left(\frac{\partial C}{\partial z} \right)_{z=0} \approx (1-r) K_z \left(\frac{\partial C}{\partial z} \right) \quad (7)$$

where v_g is the actual settling velocity, p is the deposition velocity, and r is the reflection coefficient. Varying the value of r from 0 to 1 will simulate the effect of losses at the surface by deposition (Rao, [12]).

To eliminate irregularity of the surface, the following

changes of variables are made:

$$\begin{aligned}\tau &= t, \quad \underline{X} = x_W - x_E, \quad \underline{Y} = y_N - y_S \\ \xi &= \frac{x - x_E}{\underline{X}}, \quad \underline{Z} = H - h(x, y) \\ \eta &= \frac{y - y_S}{\underline{Y}}, \quad \rho = \frac{Z - h(x, y)}{\underline{Z}}\end{aligned}\tag{8}$$

A similar change of variables was performed by Reynolds, et al, [10]. After some algebra, Equation 1 becomes

$$\begin{aligned}\frac{\partial C}{\partial \tau} + \frac{U}{\underline{X}} \frac{\partial C}{\partial \xi} + \frac{V}{\underline{Y}} \frac{\partial C}{\partial \eta} + \frac{\tilde{W}}{\underline{Z}} \frac{\partial C}{\partial \rho} &= \frac{1}{\underline{X}^2} \frac{\partial}{\partial \xi} \left[K_x \left(\frac{\partial C}{\partial \xi} \right) - \Lambda_\xi \left(\frac{\partial C}{\partial \rho} \right) \right] \\ &- \frac{\Lambda_\xi}{\underline{X}} \frac{\partial}{\partial \rho} \left[\frac{K_x}{\underline{X}} \left(\frac{\partial C}{\partial \xi} \right) - \Lambda_\xi \left(\frac{\partial C}{\partial \rho} \right) \right] \\ &+ \frac{1}{\underline{Y}^2} \frac{\partial}{\partial \eta} \left[K_y \left(\frac{\partial C}{\partial \eta} \right) - \Lambda_\eta \left(\frac{\partial C}{\partial \rho} \right) \right] \\ &- \frac{\Lambda_\eta}{\underline{Y}} \frac{\partial}{\partial \rho} \left[\frac{K_y}{\underline{Y}} \left(\frac{\partial C}{\partial \eta} \right) - \Lambda_\eta \left(\frac{\partial C}{\partial \rho} \right) \right] + \frac{1}{\underline{Z}^2} \frac{\partial}{\partial \rho} \left[K_z \frac{\partial C}{\partial \rho} \right] + S \cdot \underline{Z}\end{aligned}\tag{9}$$

where

$$\begin{aligned}\Lambda_\xi &= \frac{1}{\underline{Z}} \left(\frac{\partial h}{\partial \xi} + \rho \frac{\partial Z}{\partial \xi} \right) \\ \Lambda_\eta &= \frac{1}{\underline{Z}} \left(\frac{\partial h}{\partial \eta} + \rho \frac{\partial Z}{\partial \eta} \right) \\ \tilde{W} &= w - \frac{U}{\underline{X}} \Lambda_\xi \underline{Z} - \frac{V}{\underline{Y}} \Lambda_\eta \underline{Z}\end{aligned}\tag{10}$$

The use of Equation 8 alters the physical domain from dimensional to non-dimensional scales which vary from 0 to 1, permitting the solution to be independent of local site characteristics.

A subjective analysis and interpolation scheme is used to

calculate a first guess wind field throughout the three-dimensional region based on available data, i.e., wind speeds and directions obtained from instrumented towers. The wind field is then checked to determine mass consistency throughout the three dimensional domain. A mass consistent wind field model is used to calculate corrections to the interpolated wind vectors at each node point such that

$$\frac{\partial U'}{\partial \xi} + \frac{\partial V'}{\partial \eta} + \frac{\partial \tilde{W}}{\partial \rho} = 0 \quad (11)$$

where \tilde{W} is given by Equation 10, $U' = \underline{UZ}$ and $V' = \underline{VZ}$. Based on the technique used by Dickerson [13] and Sherman [14], a Sasaki variational treatment of the continuity Equation 14 is performed such that the integral (I)

$$I = \int \left[\alpha_1^2 (U' - U'_0)^2 + \alpha_1^2 (V' - V'_0)^2 + \alpha_2^2 (\tilde{W} - \tilde{W}_0)^2 + \lambda \left(\frac{\partial U'}{\partial \xi} + \frac{\partial V'}{\partial \eta} + \frac{\partial \tilde{W}}{\partial \rho} \right) \right] d\xi d\eta d\rho \quad (12)$$

is minimized. The constant α_1 is defined as $\alpha_1 = 1/2\sigma_1^2$ where σ_1^2 is the error variance of the horizontal velocities. The constant α_2 is defined as $\alpha_2 = 1/2\sigma_2^2$, where σ_2^2 is the error variance in the vertical velocity. U'_0 , V'_0 , and \tilde{W}_0 are the interpolated velocities, and λ is the Lagrangian multiplier and is a function of ξ , η , and ρ . Minimization of Equation 12 is accomplished when the Euler equations of I vanish. The Euler equations are given as

$$U' = U'_0 + \frac{1}{2\alpha_1^2} \frac{\partial \lambda}{\partial \xi}$$

$$V' = V_0' + \frac{1}{2\alpha_1^2} \frac{\partial \lambda}{\partial \eta}$$

$$\tilde{W} = \tilde{W}_0 + \frac{1}{2\alpha_2^2} \frac{\partial \lambda}{\partial \rho} \quad (13)$$

The unknown Lagrangian multipliers are obtained by combining Equation 13 with Equation 11. This gives the equation

$$\frac{\partial^2 \lambda}{\partial \xi^2} + \frac{\partial^2 \lambda}{\partial \eta^2} + \frac{\alpha_1^2}{\alpha_2^2} \frac{\partial^2 \lambda}{\partial \rho^2} = 2\alpha_1^2 \left(\frac{\partial U_0'}{\partial \xi} + \frac{\partial V_0'}{\partial \eta} + \frac{\partial \tilde{W}_0}{\partial \rho} \right) \quad (14)$$

Solutions for λ from Equation 14 are then used in Equation 13 to give the final adjusted wind vectors. If $(\alpha_1/\alpha_2)^2 \rightarrow \infty$, more weight is given to adjustment of the vertical velocity field. Conversely, as $(\alpha_1/\alpha_2)^2 \rightarrow 0$, more weight is given to adjustment of the horizontal velocity field. Reasonable horizontal and vertical adjusted fluxes have been obtained by Dickerson [13] and Sherman [14] if $(\sigma_2/\sigma_1)^2$ is in the neighborhood of 10^{-4} .

A great deal has yet to be understood about the nature of turbulence under variable conditions. The problem of specification of the vertical diffusion coefficient, K_z , is particularly important to the dispersion of pollutant within the mixed layer. Little is known about the behavior of K_z except near the earth's surface (Shir and Shieh, [15]; Pasquill, [16]; Tennekes and Lumley, [17]). Horizontal diffusion is generally of secondary importance in atmospheric dispersion problems

due to the predominance of the horizontal advection terms in the governing equation. However, atmospheric stability has great influence on the generation and decay of turbulence (K_z) in the atmosphere. Hence, the effect of temperature (or density) stratification must also be known. Unfortunately, sparsity of atmospheric field data hinders verification of more sophisticated closure schemes.

Based on Yu's [18] analysis of 14 different models for determining the vertical diffusion coefficient, an O'Brien [19] K-theory model is used in conjunction with similarity theory. Surface similarity theory calculates K_z from the Monin-Obukhov universal relations with measured wind velocities and temperatures from an instrumented TV tower in the transition layer region ($Z \sim 60$ m). The O'Brien cubic profile then calculates the vertical diffusivity between the transition layer region and the top of the mixing layer. This procedure was used by Pepper and Kern [20] to model atmospheric dispersion with linear finite element and cubic spline methods.

A set of universal functions, ϕ_M and ϕ_T , must be supplied along with the Obukhov atmospheric stability length, L , to obtain the vertical exchange coefficients in the transition layer. These parameters are functions of the derivatives of temperature, wind velocity, and humidity. Likewise, temperature and velocity friction values at the surface, θ^* and U^* , are also unknowns.

Atmospheric stability conditions greatly influence these parameters; one set of empirical relations is used for unstable atmospheres, while a different set is used for stable atmospheres. Hence, two general sets of relations must be solved to account for the transition from one stability category to the other. An efficient technique has been devised for solving this system of equations by Long and Shaffer [21]. The integrated profile relations are solved by a pseudo-parameter which combines the velocity gradients with the temperature gradients (analogous to the relationships used by Businger, et al., [22]) such that the stability length, L , can be calculated in a rapidly converging iteration sequence. Once L is known, θ^* , U^* , and the remaining unknown derivatives can be easily solved.

K_M and K_T (exchange coefficients for momentum and heat, respectively) are then solved from the relations

$$\begin{aligned}
 K_M &= \frac{\kappa U^* Z}{\phi_M(Z/L)} \\
 K_T &= \frac{\kappa U^* Z}{\phi_T(Z/L)}
 \end{aligned}
 \tag{15a}$$

where κ is von Karman's constant with $\phi_M(Z/L)$ and $\phi_T(Z/L)$ determined from empirical relations and the iteration scheme. In unstable conditions, $K_H > K_M = K_Z$ is used for the vertical exchange coefficients, while $K_H = K_Z > K_M$ is used in stable conditions. Equation 15a is assumed to be valid up to a physical height $Z = 62$ m (stack height). At the 62-m height, the O'Brien

[19] cubic profile is used to generate K_Z values, such that K_Z reaches a maximum above the 62-m height and gradually decreases to $0.1 \text{ m}^2 \text{ sec}^{-1}$ at the top of the mixed layer. The O'Brien cubic profile is

$$K_Z = K_{Z_{62}} + \left(\frac{Z-H}{H-62} \right)^2 \left\{ K_{Z_{62}} - K_{Z_H} + (Z-62) \left[\left(\frac{\partial K_Z}{\partial Z} \right)_{62} + \frac{2(K_{Z_{62}} - K_{Z_H})}{H-62} \right] \right\} \quad (15b)$$

Vertical mesh spacing is based on the vertical spacing of the instruments located on the TV tower and the height of the mixed layer. Ten levels are normally used with Z values set to heights of 2 m, 10 m, 36 m, 62 m, 137 m, 243 m, and 335 m; the remaining three levels are equally incremented according to the height of the mixed layer.

Horizontal diffusion for plumes and puffs is determined

as follows: (1) plumes: $K_x = K_y = \frac{1}{2} \frac{d\sigma_y^2}{dt}$ with $\sigma_y = \alpha \sigma_a X^\beta$

where α and β are constants selected in accordance with Pasquill [16] type stability categories; σ_a is the standard deviation of the azimuthal wind fluctuation (obtained from TV tower data) - in the absence of σ_a , $\sigma_y = \alpha(Ut)^\beta$ (Lange, [23]); (2) puffs:

$K_x = K_y = \epsilon^{1/3} \sigma_y^{4/3}$ where ϵ is the turbulent eddy dissipation rate based on stability category (Crawford, [24]).

The Numerical Model

In order to overcome excessive core requirements, Equation 9 is split into a series of one-dimensional equations by the method of fractional steps, (Yanenko [5]). The method of fractional steps has been used by Long and Shaffer [21], Long and Pepper [25], Reynolds et al., [10], and Pepper and Kern [20] in modeling multi-dimensional transport. Equation 9 is divided into a set of equations which are integrated in succession over one time step. Upon completion of the integrations, the full three dimensional equation is solved over one time step. Equation 9 is split into the following series of equations:

$$\frac{\partial C^*}{\partial \tau} + \frac{U}{\underline{X}} \frac{\partial C^n}{\partial \xi} + \frac{V}{\underline{Y}} \frac{\partial C^n}{\partial n} + \frac{\tilde{W}}{\underline{Z}} \frac{\partial C^n}{\partial \rho} = 0 \quad (16)$$

$$\begin{aligned} \frac{\partial C^{**}}{\partial \tau} = & - \frac{1}{\underline{X}^2} \frac{\partial}{\partial \xi} \left[k_x \Lambda_\xi \frac{\partial C^*}{\partial \rho} \right] - \frac{\Lambda_\xi}{\underline{X}} \frac{\partial}{\partial \rho} \left[\frac{k_x}{\underline{X}} \frac{\partial C^*}{\partial \xi} \right] \\ & - \frac{1}{\underline{Y}^2} \frac{\partial}{\partial n} \left[k_y \Lambda_n \frac{\partial C^*}{\partial \rho} \right] - \frac{\Lambda_n}{\underline{Y}} \frac{\partial}{\partial \rho} \left[\frac{k_y}{\underline{Y}} \frac{\partial C^*}{\partial n} \right] \end{aligned} \quad (17)$$

$$\frac{\partial C^{***}}{\partial \tau} = \frac{\Lambda_\xi}{\underline{X}} \frac{\partial}{\partial \rho} \left[\frac{k_x \cdot \Lambda_\xi}{\underline{X}} \frac{\partial C^{**}}{\partial \rho} \right] + \frac{\Lambda_n}{\underline{Y}} \frac{\partial}{\partial \rho} \left[\frac{k_y \cdot \Lambda_n}{\underline{Y}} \frac{\partial C^{**}}{\partial \rho} \right] \quad (18)$$

$$\begin{aligned} \frac{\partial C^{n+1}}{\partial \tau} = & \frac{1}{\underline{X}^2} \frac{\partial}{\partial \underline{\xi}} \left[K_x \frac{\partial C^{***}}{\partial \underline{\xi}} \right] + \frac{1}{\underline{Y}^2} \frac{\partial}{\partial \eta} \left[K_y \frac{\partial C^{***}}{\partial \eta} \right] \\ & + \frac{1}{\underline{Z}^2} \frac{\partial}{\partial \rho} \left[K_z \frac{\partial C^{***}}{\partial \rho} \right] \end{aligned} \quad (19)$$

Successive solutions to Equations 16 through 19 give the final solution to Equation 9 at one time step.

Fortunately, Equation set 16-19 can be reduced to only Equations 16 and 19 under most conditions. If changes in ground elevation are gradual (as they are around SRP), the derivatives $\partial h/\partial \underline{\xi}$, $\partial h/\partial \eta$, $\partial \underline{Z}/\partial \underline{\xi}$, and $\partial \underline{Z}/\partial \eta$ are small compared to other terms in the equation set. Hence, the diffusion terms containing $\Lambda_{\underline{\xi}}$ and Λ_{η} (Equations 17 and 18) are neglected. Although there is some error in deleting these terms when the terrain is highly irregular, Equations 17 and 18 involve only horizontal diffusion, which is generally negligible in comparison to horizontal advection. Thus, the total error incurred is considered to be minimal (results obtained with the entire equation set versus results obtained with only Equations 16 and 19 were nearly identical).

In an effort to minimize numerical errors, the three-dimensional method-of-moments is used to calculate the advection of pollutant concentration, Equation 16. This method is based on the calculation of moment distributions

of a concentration within a cell, (Egan & Mahoney [1]).

The method calculates the zeroth, first, and second moments of the concentration within a mesh and then advects and diffuses the concentration by maintaining conservation of the moments. The moments correspond to the mean concentration, center of mass, and scaled distribution variance (moment of inertia), respectively, and are given by

$$C_i = \int_{-0.5}^{0.5} C(\xi_i) d\xi \quad (20)$$

$$F_i = \int_{-0.5}^{0.5} C(\xi_i) \xi_i d\xi / C_i \quad (21)$$

$$R_i^2 = 12 \int_{-0.5}^{0.5} C(\xi_i) (\xi_i - F_i)^2 d\xi / C_i \quad (22)$$

where ξ_i denotes the relative displacement of material within the i^{th} cell from the center of the cell. ξ_i varies from -0.5 to +0.5 corresponding to the left and right hand extreme boundaries of a cell. The length dimensions of the cell are non-dimensionalized by the grid element length (width or height, depending on the direction of calculation). For simple rectangular concentration distributions, i.e., rectangular mesh geometry, the integrals can be readily evaluated by summation for each grid element in terms of the concentration

distributions of the portions remaining and newly transported for each successive time step. The advection of a single cell of concentration is shown in Figure 1. The single cell of concentration is advected accurately with time and without numerical dispersion or computational damping errors. The advection of a single cell of concentration in two dimensions is shown in Figure 2 with similar results. Further tests with two and three dimensional advection of both single and multiple cells of concentration showed no numerical dispersion errors and minimal damping (Pepper and Long, [4]).

Tests on hyperbolic equations with both finite difference and finite element techniques by Long and Pepper [25] and Baker, et al., [26] showed either severe spreading of the concentration (due to computational damping) or generation of wave (plus and minus) packets of concentration (due to numerical dispersion). Since the immediate dispersion of concentration is essentially one of advection, the second moment method is amply suited for the solution of the three-dimensional equation of concentration transport.

The downwind transfer of concentration by advection depends upon the value of the portioning parameter, P_i , where P_i is defined as

$$P_i = \left(F_i + \gamma + \frac{R_i}{2} - 0.5 \right) / R_i \quad (23)$$

where γ is the Courant number. If $P_i < 0$, none of the concentration is advected into the $i+1$ cell. If $P_i > 0$, all of

the concentration is advected into the downwind cell. For $0 < P_i < 1$, a fraction of the concentration $P_i C_i$ is advected while $(1-P_i) C_i$ remains behind. Figure 3 shows the scaling parameters involved in the advection of a rectangular concentration distribution during one time step. The center of mass of the distribution (for one dimensional advection) is given at $(-0.5 + P_i R_i / 2)$ relative to the center of the $i + 1$ cell and has a horizontal spread equal to P_i / R_i in the new cell. The amount left in cell i has a center of mass at $(1 - R_i + P_i R_i) / 2$ with a horizontal spread of $(1 - P_i) R_i$.

Extension of the method of moments to two and three dimensions is straightforward as based on the rules for the one dimensional example just discussed. The zeroth through second moments are evaluated from concentration distributions advected from several adjacent cells in multi-dimensional flow. The computational procedure then determines which neighboring cells contribute to the moment calculation and computes the new values for each cell. Thus, the moment distributions are calculated using

$$C^{n+1} = \Sigma C_i \quad (24)$$

$$F^{n+1} = \frac{\Sigma C_i F_i}{C^{n+1}} \quad (25)$$

$$R^2 \Big)^{n+1} = \frac{\Sigma C_i R_i^2}{C^{n+1}} + 12 \Sigma C_i \left(F_i - F_i^{n+1} \right)^2 \quad (26)$$

where $n+1$ denotes values at the new time step and m denotes cell location in the computational mesh.

Equation 19 is solved using cubic splines. Cubic spline methods have been used by Price and MacPherson [6], Chawla, et al., [27], Rubin and Khosla [28], Rubin and Graves [7], Purnell [29], Long and Pepper [25], and Pepper and Kern [20]. The spline representation in a Galerkin method has been used by Hsu [30] in solving boundary layer flow problems. Variable interpolation schemes using cubics and quintics were also analyzed by Price, et al. [31]. High order accuracy was likewise obtained in solving the one-dimensional advection-diffusion equation.

The method of cubic splines can best be demonstrated through solution of the simple one-dimensional advection-diffusion equation

$$\frac{\partial C}{\partial t} + U \frac{\partial C}{\partial x} - K \frac{\partial^2 C}{\partial x^2} = 0 \quad (27)$$

By writing the time dependent derivative as a forward-in-time difference term and the spatial derivatives as a cubic spline passing through grid point, x_i , Equation 27 can be rewritten as

$$\frac{C_i^{n+1} - C_i^n}{\Delta t} + U_i^n f_i - K S_i = 0 \quad (28)$$

where the first derivative has been replaced by the unknown variable f_i and the second derivative by S_i . Based on the procedure outlined by Rubin and Graves [7], f_i and S_i are written as tri-diagonal relations

$$\begin{aligned} \frac{f_{i-1}}{\Delta x_-} - 2 \left(\frac{1}{\Delta x_-} + \frac{1}{\Delta x_+} \right) f_i + \frac{f_{i+1}}{\Delta x_+} \\ = 3 \frac{(C_{i+1} - C_i)_+}{\Delta x_+^2} + 3 \frac{(C_i - C_{i-1})_-}{\Delta x_-^2} \end{aligned} \quad (29)$$

$$\begin{aligned} \frac{\Delta x_-}{6} S_{i-1} + \frac{\Delta x_- + \Delta x_+}{3} S_i + \frac{\Delta x_+}{6} S_{i+1} \\ = \frac{C_{i+1} - C_i}{\Delta x_+} - \frac{C_i - C_{i-1}}{\Delta x_-} \end{aligned} \quad (30)$$

where $\Delta x_- = x_i - x_{i-1}$ and $\Delta x_+ = x_{i+1} - x_i$. If the right hand side values are known, solutions for f_i and S_i can be easily found using a tri-diagonal inversion algorithm.

The boundary conditions associated with Equations 29 and 30 specify that either f_i or S_i is equal to a known value or is set equal to zero. This particular feature of cubic spline methods is advantageous over more conventional finite difference boundary value approximations (particularly first order forward-in-space differences). The spline derivatives at a point are linked to their neighbors in a global sense by their tri-diagonal nature. Equations 29 and 30 are somewhat analogous to linear finite element basis functions assembled over adjacent nodes [20].

Equation 19 is solved in the following way:

$$1) \text{ Let } m_i = K_z \left. \frac{\partial C^{***}}{\partial \rho} \right|_i$$

2) Solve for m_i

$$\begin{aligned} \frac{m_{i-1}}{\Delta\rho} + 2 m_i \left(\frac{1}{\Delta\rho_-} + \frac{1}{\Delta\rho_+} \right) + \frac{m_{i+1}}{\Delta\rho_+} \\ = \frac{3}{\Delta\rho_+^2} (C_{i+1} - C_i) + \frac{3}{\Delta\rho_-^2} (C_i - C_{i-1}) \end{aligned} \quad (31)$$

3) Once m_i is obtained, let $\ell_i = \frac{1}{Z^2} \frac{\partial m_i}{\partial \rho}$

4) Solve $\frac{C_i^{n+1} - C_i^{***}}{\Delta t} - \ell_i = 0$

5) Repeat steps 1-4 for the remaining horizontal diffusion terms.

If the diffusion coefficient is constant, the single tri-diagonal relation for the second derivative term is more efficient to use, Equation 30. (If the advection terms are zero and the problem is one of only diffusion, the cross derivative terms appearing in Equations 17 and 18 can be solved using two first derivative cubic spline relations in succession.)

To maintain conservation of the zeroth, first, and second moment distribution, the moments are recalculated after Equation 19 is solved. The first and second moments are recalculated by the following general relations (using the one dimensional example for vertical diffusion):

$$\begin{aligned}
F_k^{n+1} &= \left[C_k^n F_k^n \left(1 - \alpha_{k+1} - \alpha_{k-1} \right) + \alpha_{k+1} C_{k+1}^n + F_{k+1}^n \right. \\
&\quad \left. + \alpha_{k-1} C_{k-1}^n F_{k-1}^n \right] / C_k^{n+1} \\
(R_k^2)^{n+1} &= \left\{ C_k^n \left[(R_k^2)^n + 12 \left(F_k^n - F_k^{n+1} \right)^2 \right] \left(1 - \alpha_{k+1} - \alpha_{k-1} \right) \right. \\
&\quad + \alpha_{k+1} C_{k+1}^n \left[(R_{k+1}^2)^n + 12 \left(F_{k+1}^n - F_{k+1}^{n+1} \right)^2 \right] \\
&\quad + \alpha_{k-1} C_{k-1}^n \left[(R_{k-1}^2)^n + \right. \\
&\quad \left. \left. + 12 \left(F_{k-1}^n - F_{k-1}^{n+1} \right)^2 \right] \right\} / C_k^{n+1} \tag{33}
\end{aligned}$$

To further enhance resolution of the peak concentration and to prevent unwanted (or inaccurate) horizontal spread, a slightly modified version of the second moment solution is used. Based on the technique developed by Pedersen and Prahm [2], a width correction procedure is used to check the lateral spread of concentration within each cell. If R_i^{n+1} is greater than $F_i^{n+1} \pm 0.5$, then $R_i^{n+1} = \min \left| F_i^{n+1} \pm 0.5 \right|$. This procedure reduces the small amounts of lateral dispersion errors produced from a nonuniform concentration field and an irregular flow field. A detailed account of the effect of the width correction procedure on the second moment method under variable conditions is given by Pepper and Long [4].

Equation 14 is solved by a three dimensional strongly implicit procedure (SIP). SIP, first developed by Stone [32], has been used predominantly to calculate two dimensional

viscous flow problems (Bozeman and Dalton, [33]; Jacobs, [34]; Lin, et al., [35]; and Pepper and Harris, [36]). SIP has also been used to model time-dependent, mesoscale concentrations in two dimensions by Pepper and Kern [37]. The three dimensional SIP has been used by Weinstein, et al., [38] for multi-phase reservoir flow problems and by Long and Pepper [25] to calculate atmospheric advection of concentration. Pepper and Harris [39] have used a three-dimensional SIP to calculate free convective flow in a closed container.

SIP requires Equation 14 to be separated into discrete finite differences by forward in time, centered in space approximations for the derivative terms. The separation creates a sparse matrix banded by seven diagonal elements.

The discretized form of Equation 14 is written as

$$\begin{aligned}
 D \lambda_{i-1,j,k}^{n+1} + F \lambda_{i+1,j,k}^{n+1} + B \lambda_{i,j-1,k}^{n+1} + H \lambda_{i,j+1,k}^{n+1} \\
 + T \lambda_{i,j,k-1}^{n+1} + S \lambda_{i,j,k+1}^{n+1} + E \lambda_{i,j,k}^{n+1} \\
 = q_{i,j,k}^n
 \end{aligned} \tag{34}$$

where the coefficients D, F, B, H, T, S, E, and q are defined as

$$D = 2/((\Delta\xi_+ + \Delta\xi_-)\Delta\xi_-)$$

$$F = 2/((\Delta\xi_+ + \Delta\xi_-)\Delta\xi_+)$$

$$B = 2/((\Delta\eta_+ + \Delta\eta_-)\Delta\eta_-)$$

$$H = 2/((\Delta\eta_+ + \Delta\eta_-)\Delta\eta_+)$$

$$T = 2 \cdot (\alpha_1^2/\alpha_2^2)/((\Delta\rho_+ + \Delta\rho_-)\Delta\rho_-)$$

$$S = 2 \cdot (\alpha_1^2/\alpha_2^2)/((\Delta\rho_+ + \Delta\rho_-)\Delta\rho_+)$$

$$E = -2/(\Delta\xi_+ + \Delta\xi_-)^2 - 2/(\Delta\eta_+ + \Delta\eta_-)^2 - 2(\alpha_1^2/\alpha_2^2)/(\Delta\rho_+ + \Delta\rho_-)^2 \quad (35)$$

$$q_{i,j,k} = 2\alpha_1^2 (f_{x_0} + f_{y_0} + f_{z_0})$$

where $\Delta\xi_+ = s_{i+1} - s_i$, $\Delta\xi_- = s_i - s_{i-1}$, $\Delta\eta_+ = \eta_{j+1} - \eta_j$, etc.

The terms f_{x_0} , f_{y_0} , and f_{z_0} represent the continuity equation first derivatives

$$f_{x_0} \equiv \frac{\partial U_0}{\partial \xi}, \quad f_{y_0} \equiv \frac{\partial V_0}{\partial \eta}, \quad \text{and} \quad f_{z_0} \equiv \frac{\partial W_0}{\partial \rho}$$

These first derivative terms are obtained from the interpolated wind vectors using the cubic spline relation given by Equation 29.

Equation 34 can be rewritten in matrix form as

$$[M] \{\lambda\} = \{q\} \quad (36a)$$

where $[M]$ is the sparse coefficient matrix containing seven diagonals, $\{\lambda\}$ is the column matrix of unknown values of the Lagrangian multipliers, and $\{q\}$ is the column matrix of explicitly known values (term evaluated at the n^{th} iterative step). SIP alters matrix $[M]$ from a seven diagonal matrix to a 13 diagonal matrix $[M']$. This allows matrix $[M']$ to be factored into a series of lower and upper diagonal matrices, $[L]$ and $[U]$, which can be efficiently solved by elimination techniques.

The three-dimensional SIP algorithms are discussed in more detail by Weinstein, et al. [38] and Pepper and Harris [39]. Round-off errors are reduced by solving $\{\lambda\}$ values in residual form such that

$$[M']\{\Delta\lambda^{n+1}\} = \{R\} \quad (36b)$$

where $\{R\} = \{q\} - [M]\{\lambda\}$ and $\Delta\lambda^{n+1} = \lambda^{n+1} - \lambda^n$. Once $\Delta\lambda^{n+1}$ is solved, λ^{n+1} can be obtained. Weinstein, et al [39] compared the accuracy of SIP with an ADI procedure, and found that: single precision SIP solutions were comparable to double precision ADI solutions; SIP is less sensitive to rounding errors than ADI procedures; and although SIP requires larger iteration time than ADI, fewer iterations are needed to converge the solution. Similar studies made by Lin, et al. [35] and Pepper and Harris [36] support these observations. Readjustment of the interpolated wind field to a mass consistent wind field required only a few iterations.*

The initial dispersion of emissions from point or area sources can be either user input according to the cell volume source or obtained using a Gaussian puff/plume format. Pasquill [16] established that the Gaussian puff/plume analytical solution of Equation 1 gives reliable results to a distance of several kilometers from the source. Beyond this distance, the variability of the wind field with time, as well as the three dimensional nature of the winds (particularly in rough terrain where recirculation or flow separation may occur) severely limits the applicability of the analytical solution.

*Direct solutions using cyclic-reduction, fast-Fourier transform methods can also effectively solve Equation 14.

However, by incorporating the contributions from a point source into the numerical advection scheme, the three dimensional model can accurately maintain the subgrid resolution of the emission within a grid element. Best results are obtained when the puff or plume has grown large enough to be approximated by a few shallow regions of uniform concentration.

The computational domain consists of 10,890 cells; 33 cells in the longitudinal direction (ξ), 33 cells in the lateral direction (η), and 10 levels in the vertical direction (ρ). Mesh spacing can either be arbitrarily set (such as telescoping grid network) or equally spaced with $\Delta\xi = \Delta\eta$. The vertical mesh spacing is based on the ground level values for topography ($Z_0 = h(x,y)$) and the height of the lid ($Z_{10} = H$). User input values for the remaining levels, i.e., levels corresponding to instrumented tower locations, are automatically transformed to non-dimensional values such that $0 < \rho < 1$ throughout the computational domain. The stability criteria, $\gamma_i < 1$,* is satisfied by checking γ_i at every time step. If $\gamma_i > 1$, the time step, Δt , is reduced such that $\gamma_i < 1$. This stability criteria must be met since the advection scheme is explicit.

If the height of the mixed layer, H , varies with time, ($H = H(x,y,z,t)$), a slightly more detailed computational sequence must be used since derivatives of H would appear throughout the equation. The computational procedure is solved using the JOSHUA data management system employed at

* $\gamma_i \equiv \gamma_x = U\Delta t/\Delta x, \gamma_y = V\Delta t/\Delta y, \gamma_z = W\Delta t/\Delta z$

SRL (Honeck, [40]). The JOSHUA network allows the computational modules to be efficiently handled without significant storage problems. A typical problem of a release, calculated within the computational domain, requires approximately 480 K bytes. Computational running times are generally under two minutes on an IBM-360/195 for a real time simulation of several hours. Optimization of the code would likely reduce storage requirements as well as speed up computation. The JOSHUA network is coupled with a PDP-1140 minicomputer which accumulates real time data from the tower network at SRP. The coupling allows the vector wind field and concentration isopleths to be simultaneously displayed on a cathode ray tube per time step.

Horizontal Wind Fields Over SRP

Surface meteorological observations are available hourly from the National Weather Service stations in the southeastern United States. Twice-a-day, upper-atmospheric observations are available from Athens, Georgia, and Charleston, South Carolina, (SRP lies on a line about half-way between these two stations). Wind speed data, bivane direction data, and temperature data are available from various levels up to 335 m from sensors mounted on the WJBF-TV tower located near SRP. The wind speed and bivane direction data are also available from seven 62-m towers located at the production

areas of the SRP (Figure 4). The SRP and the National Weather Service stations in the southeastern United States provide the initial and boundary condition data for the analyses used as input to the transport and diffusion model.

Gridded analyses are derived from the data to provide fields of wind vectors over three nests of grids. The analysis technique uses a scan radius determined by the density of the data. Data influencing, grid-point values are proportional to the exponential of the inverse square of the distance between the data and grid point (Fleming, [41]).

The three nests of grids, all centered on SRP, contain 33×33 grid points and are sub-sets of the National Weather Service's National Meteorological Center (NMC) square, polar stereographic, computational grid. The largest grid has a grid spacing of $1/8$ the NMC grid (for a grid separation of about 40 km). The next nest has a grid spacing of $1/32$ of the NMC grid, (or a spacing of about 10 km). The smallest grid has a grid spacing of $1/128$ of the NMC grid (or a 2.5 km separation). The smallest grid (used for these calculations) can be uniform or nonuniform. The largest grid is used to obtain the best first guess for the next smaller grid and to incorporate the maximum amount of National Weather Service synoptic data. The 10 km grid analysis provides the first guess for the small grid nest. Concentration calculations are performed using the wind fields of the small grid nest.

RESULTS

To assess numerical accuracy, a simple test was conducted using six cell sources, each with a unit release advected in a two dimensional wind field. Figure 5 compares results of the numerical model with those of an analytical solution (Pederson and Prahm, [2]). The results are nearly identical. The computed peak centerline values as well as the width of the plume are accurately maintained. All remaining values in the computational domain are zero (simple finite difference procedures tend to produce wider plume width with less centerline concentration). Results are also identical to numerical values obtained by Pedersen and Prahm [2] using a two dimensional method of moments. In both methods, a width correction procedure has been used to eliminate small amounts of lateral dispersion at the plume edge, [4].

A test of two dimensional advection-diffusion in the x-y plane is shown in Figure 6 for a continuous area source emission consisting of four cells each containing 250 units. Analytical results (assuming Fickian diffusion) were obtained from Christensen and Prahm [42]. Lateral diffusion (K_y) was set equal to 0.10 with $K_x = K_z = 0$. Advection occurred only in the longitudinal direction (ξ) with $U = 1$, $V = W = 0$. An identical comparison was made by Christensen and Prahm [42] using a pseudospectral method. Cell values obtained by the numerical model agree reasonably well with cell values obtained from the analytical model. Peak centerline values are predicted

by the numerical model within 3 percent (average) of the analytical values. The lateral spread of concentration is nearly identical, deviating by only a few percent in each individual cell value.

The effect of surface irregularity on a continuous elevated emission is shown in Figures 7-9. Figure 7 shows the elevation distribution of the ground plane; a continuous release was assumed to occur at a height of 200 m at the left-center cell (denoted with a dot). A 200 m peak surface elevation occurs 11 km downwind. The height of the lid is constant at 650 m. Equal grid spacing is used in the x-y plane spanning a 400 km² area, with $\Delta X = \Delta Y = 1000$ m; vertical grid spacing is equally incremented in 100 m intervals. A continuous emission rate of 1 gm/sec (Q) is used. Atmospheric stability conditions are assumed to be neutral: $K_y = 33$ m²/sec throughout the domain and $K_z = f(z)$ (K_y and K_z obtained from Pasquill stability curves at 1000 m distances (Slade, [43] - Chapter 3)). The initial velocity field is given as

$$U = 5.0 \left(\frac{z}{.2} \right)^{.14}$$

$$V = W = 0 \quad (37)$$

Hence, at a source elevation of 200 m, the velocity field is given as $\vec{U}_{200} = (13.15, 0, 0)$ m/sec.

Concentration isopleths and the computed mass-consistent, vector-wind field are shown in Figure 7 in the midplane of the computational domain. The length of an individual wind

vector denotes the magnitude of the wind speed.* The wind field is held constant after readjustment and concentration isopleths are drawn for steady state conditions. For steady state, non varying winds ($\vec{U} = 13.15, 0, 0$) m/sec, and flat surfaces, concentration isopleths generally become smoothly distributed throughout the vertical plane. Topography causes the vertical distributions to be perturbed at locations corresponding to surface peaks.

The effect of topography is more evident in Figure 9 where ground level centerline C/Q values are plotted as a function of longitudinal distance. The analytical solution was obtained from the relation (Kao, [44])

$$C = \frac{U}{2\pi U \sigma_y(x) \sigma_z(x)} e^{-\frac{y^2}{2\sigma_y^2(x)}} e^{-\frac{(Z-\tilde{H})^2}{2\sigma_z^2(x)}} \left(e^{-\frac{[Z+\tilde{H}-2h(x,y)]^2}{2\sigma_z^2(x)}} \right) \quad (38)$$

where $\sigma_y^2(x) = 2K_y t$, $\sigma_z^2(x) = 2K_z t$, \tilde{H} is the height of release, $h(x,y)$ is the height of the topographic surface, and $Z > h(x,y)$. For ground level centerline values and $Q = 1$ gm/sec, Equation 38 reduces to

$$C = \frac{1}{2\pi U \sigma_y \sigma_z} e^{-\frac{(h-\tilde{H})^2}{2\sigma_z^2}} e^{-\frac{(\tilde{H}-h)^2}{2\sigma_z^2}} \quad (39)$$

*Vertical scale increased to enhance visualization of small vertical velocities.

For ground level centerline values without topography, Equation 39 reduces to the standard Gaussian plume formula

$$C = \frac{1}{\pi U \sigma_y \sigma_z} \left(e^{-\frac{\tilde{H}^2}{2\sigma_z^2}} \right) \quad (40)$$

Relations used for the standard deviations σ_y and σ_z are conjectural. However, to be consistent in the comparison, σ_y and σ_z values are calculated from K_y and K_z values as in the numerical model (under more realistic conditions, σ_y and σ_z values could be determined as a function of longitudinal distance - Smith, [45]). Peak ground level values occur at locations corresponding to surface peaks, contrary to the smooth profile given by Equation 40. Centerline values are approximately an order of magnitude greater than values obtained without inclusion of topography.

The final test case corresponds to prediction of an actual release of tritium from the Savannah River Plant (SRP) for which experimental data are available. Averaged over the four-minute release period, tritium was present in the exhaust air at a concentration of approximately 13 ppm by volume. Because of this low dilution, the discharge was assumed to behave as a neutral gas with no buoyancy. At the time of the release, a polar front was located approximately 80 km north of SRP (Figure 10). This front represented a dividing line between two different wind fields present in the Carolinas during and after the release. Winds below the front were predominantly from the southwest. Sky conditions were generally overcast with precipitation north of the front.

The vector wind field and initial concentration distribution at the 62-m height over SRP are shown in Figure 11. The overcast skies and generally steady winds produced atmospheric diffusion corresponding to Pasquill Category D (slightly stable). Measurements obtained with an acoustic sounder indicated that the height of the mixed layer was approximately 610 m. Hence, the concentration puff was assumed to be transported and diffused by the wind field below this height. The solution was initiated with the source term set equal to 4.79×10^5 Ci. Wind field data provided hourly by the National Weather Service and the meso-tower network was used to update the mass consistent vector wind field.

The measured concentration and prediction of the model at ground level at 1255 EDT are shown in Figure 12. The calculated ground level concentration of 241,000 pCi/m³ at Springfield, South Carolina, is within 38 percent of the experimentally measured value (389,000 pCi/m³). For comparison, a Gaussian puff analytical model predicted a ground level concentration of 150,000 pCi/m³; to within 69 percent of the experimental value.

CONCLUSIONS

The three-dimensional, time-dependent equation of pollutant transport is calculated using three-dimensional second moments for advection and cubic splines for diffusion. The method of moments is a unique quasi-Lagrangian advection scheme which

produces a minimum of computational damping errors and yields subgrid-scale resolution for pollutant concentrations within a cell volume. Three-dimensional cubic spline interpolation functions are used to calculate the first and second derivatives appearing in the diffusion terms. Both techniques are computationally efficient and relatively easy to use. The technique of fractional steps reduces computer programming complexity. Topography is incorporated into the model by transforming the governing equations such that surface irregularities in the physical domain are treated as rectangular cells in the computational domain.

Mesoscale analysis of the wind field data over SRP is obtained from the National Weather Service and a network of instrumented towers situated throughout the 770 square kilometer area of SRP. The wind data are continuously updated, and the three dimensional wind field is interpolated to all grid points. The wind field is made mass consistent by performing a Sasaki variational analysis over the entire mesh. Lagrangian multipliers are calculated with a three dimensional strongly implicit procedure. The velocity components are adjusted at each succeeding time step.

Model results agree with known analytical solutions for simple releases under ideal conditions. The three dimensional numerical results agree with analytical results for ground level values over smoothly varying terrain. The principle

advantage of the three dimensional model is its ability to calculate concentration values for variable wind conditions over complex terrain without numerical dispersion errors.

The ability of the numerical scheme to simulate an actual release from SRP was assessed by modeling the May 2, 1974, accidental release of tritium gas and calculating the trajectory for six hours. Atmospheric diffusion corresponded to nearly neutral stability. Horizontal winds were obtained from the seven tower meso network at SRP. Calculated ground level concentration at a distance of 56 km from the source was within 38 percent of the actual measure value; a Gaussian puff analytical solution gave a value within 69 percent (considered to be quite good under such ideal weather conditions). Further generalization of the computer code is being undertaken to solve water transport and engineering reactor problems.

REFERENCES

1. B. A. Egan and J. R. Mahoney. "Numerical Modeling of Advection and Diffusion of Urban Area Source Pollutants." *J. Appl. Meteor.* 11, 312 (1972).
2. L. B. Pedersen and L. P. Prahm. "A Method for Numerical Solution of the Advection Equation." p 594 in *Tellus* 26. (1974).
3. K. Fischer. "Subgrid Numerical Representations and Their Improvement of Convective Difference Schemes." p 368 in *Adv. in Computer Methods for Part Diff. Eqn's. - II*, IMACS, (1977).
4. D. W. Pepper and P. E. Long. "A Comparison of Results Using Second-Order Moments With and Without Width Correction to Solve the Advection Equation." *J. Appl. Meteor.* 17, 228 (1978).
5. N. N. Yanenko. *The Method of Fractional Steps. Solution of Problems of Mathematical Physics in Several Variables.* Springer-Verlag, Heidelberg, Germany (1971).
6. G. V. Price and A. K. MacPherson. "A Numerical Weather Forecasting Method Using Cubic Splines on a Variable Mesh." *J. Appl. Meteor.* 12, 1102 (1973).
7. S. G. Rubin and R. A. Graves, Jr. "Viscous Flow Solution with a Cubic Spline Approximation." *Comp. and Fluids.* 3, 1 (1975).
8. J. H. Ahlberg, E. N. Nilson, and J. L. Walsh. *The Theory of Splines and Their Applications*, Academic Press, New York, 284 pp (1967).
9. D. J. Fyfe. "The Use of Cubic Splines in the Solution of Two-Point Boundary Value Problems." *Comp. J.* 12 (2), 188 (1969).
10. S. D. Reynolds, P. M. Roth, and J. H. Seinfeld. "Mathematical Modeling of Photochemical Air Pollution - I: Formulation of the Model." *Atmos. Environ.* 7, 1033 (1973).
11. K. L. Calder. "The Numerical Solution of Atmospheric Diffusion Equation by Finite Difference Methods." Dept. of Armo Tech. Memo. 130 (1968).

12. K. S. Rao, 1976: Personal Communication.
13. M. H. Dickerson. *A Three-Dimensional Mass-Consistent Atmospheric Flux Model for Region with Complex Topography*. UCRL Report 76157, Lawrence Livermore Laboratory, Livermore, CA (1975).
14. C. A. Sherman. *A Mass-Consistent Model for Wind Fields over Complex Terrain*. UCRL Report 76171, Lawrence Livermore Laboratory, Livermore, CA, 35 pp (1977).
15. C. C. Shir and L. J. Shieh. "A Generalized Urban Air Pollution Model and Its Application to the Study of SO₂ Distribution in the St. Louis Metropolitan Area." *J. Appl. Meteor.* 13, 185 (1974).
16. F. Pasquill. *Atmospheric Diffusion: The Dispersion of Wind-borne Material from Industrial & Other Sources*. (2nd Edition). John Wiley and Sons, New York (1974).
17. H. Tennekes and J. L. Lunley. *A First Course on Turbulence*. MIT Press, Cambridge, Massachusetts (1972).
18. T. Yu. "A Comparative Study on Parameterization of Vertical Turbulent Exchange Processes. *Mon. Weather Rev.* 105, 57 (1977).
19. J. J. O'Brien. "A Note on the Vertical Structure of the Eddy Exchange Coefficient in the Planetary Boundary Layer." *J. Atmos. Sci.* 27, 1213 (1970).
20. D. W. Pepper and C. D. Kern. "Modeling the Dispersion of Atmospheric Pollution Using Cubic Splines and Chapeau Functions." submitted to *Atmos. Environ.* (1978).
21. P. E. Long and W. A. Shaffer. *Some Physical and Numerical Aspects of Boundary Layer Modeling*. NOAA Technical Memorandum NSW TDL-56, Technical Development Laboratory, Silver Springs, MD (1975).
22. J. A. Businger, J. C. Wyngaard, Y. Izumi, and E. F. Bradley. "Flux-Profile Relationships in the Atmospheric Surface Layer." *J. Atmos. Sci.* 28, 181 (1971).
23. R. Lange. *ADPIC: A Three-Dimensional Computer Code for the Study of Pollutant Dispersal and Deposition under Complex Conditions*. UCRL Report 51462, Lawrence Livermore Laboratory, Livermore, CA (1973).

24. T. V. Crawford. *A Computer Program for Calculating the Atmospheric Dispersion of Large Clouds*. Lawrence Radiation Laboratory, UCRL Report 50179, Lawrence Livermore Laboratory, Livermore, CA (1966).
25. P. E. Long and D. W. Pepper. "A Comparison of Six Numerical Schemes for Calculating the Advection of Atmospheric Pollution." Presented at the *Third Symposium on Atmospheric Turbulence, Diffusion and Air Quality*, October 19-22, 1976, Raleigh, NC (1976).
26. A. J. Baker, M. O. Soliman, and D. W. Pepper. "A Time Split Finite Element Algorithm for Environmental Release Prediction." Presented at *Second Int. Conf. on Finite Elements in Water Resources*, July 10-14, 1978, Imperial College, London, England (1978).
27. T. C. Chawla, et al., "The Application of Collocation Method Using Hermite Cubic Splines to Nonlinear Transient One-Dimensional Heat Conduction Problems." *Trans. ASME 97C (4)*, 562 (1975).
28. S. G. Rubin and P. K. Khosla. "Higher-Order Numerical Solutions Using Cubic Splines." *AIAA J. 14*, 851 (1976).
29. D. K. Purnell. "Solution of the Advection Equation by Upstream Interpolation with a Cubic Spline." *Mon. Weather Rev. 104*, 42 (1976).
30. C. C. Hsu. "The Use of Splines for the Solution of Boundary Layer Equations." p 129 in *Numerical/Laboratory Computer Methods in Fluid Mechanics*. ASME, NY (1976).
31. H. S. Price, J. C. Cavendish, and R. S. Varga. "Numerical Methods of High-Order Accuracy for Diffusion-Convection Equations." *Soc. Pet. Eng. J. 243 (3)*, 293 (1968).
32. H. L. Stone. "Iterative Solution of Implicit Approximations of Multidimensional Partial Differential Equations." *SIAM J. Numerical Anal. 5*, 530 (1968).
33. J. D. Bozeman and C. Dalton. "Numerical Study of Viscous Flow in a Cavity." *J. Comp. Phys. 12*, 348 (1973).
34. D. A. Jacobs. *A Corrected Upwind Differencing Scheme Using a Strongly Implicit Solution Procedure*. Pentech Press, London, England (1973).
35. C. L. Lin, D. W. Pepper, and S. C. Lee. "Numerical Methods for Separated Flow Solutions Around a Circular Cylinder." *AIAA J. 14*, 900 (1976).

36. D. W. Pepper and S. D. Harris. "Numerical Simulation of Natural Convection in Closed Containers by a Fully Implicit Method." *J. Fluid Engr.* 99 (1) 4, 649 (1977).
37. D. W. Pepper and C. D. Kern. "Modeling of Two-Dimensional Mesoscale Concentrations Using a Strongly Implicit Procedure." Presented at the *First Conference on Regional and Mesoscale Modeling, Analysis, and Prediction*, May 6-9, 1975, Las Vegas, Nevada (1975).
38. H. G. Weinstein, H. L. Stone, and T. V. Kwan. "Iterative Procedure for Solution of Systems of Parabolic and Elliptic Equations in Three Dimensions." *Indus. and Engr. Chem. Fund.* 8, 281 (1969).
39. D. W. Pepper and S. D. Harris. "Numerical Solution of Three-Dimensional Natural Convection by the Strongly Implicit Procedure." To be presented at the *1978 Winter Annual Meeting of ASME*, San Francisco, CA, Dec. 10-15, 1978
40. H. C. Honeck. *The JOSHUA System*. USERDA Report DP-1380. Available through NTIS, Fed. Clearing House, Springfield, Virginia (1975).
41. R. J. Fleming. *AFGWC Fine-Mesh Upper Air Analysis Model*. Air Force Global Weather Center Report TM-69-2, available through NTIS, Fed. Clearing House, Springfield, Virginia as AD 710203 (1969).
42. O. Christensen and L. P. Prahm. "A Pseudospectral Model for Dispersion of Atmospheric Pollutants." *J. Appl Meteor.* 15, 284 (1976).
43. D. Slade. *Meteorology and Atomic Energy*. USAEC-OIS, available through NTIS TID-24190, Fed. Clearing House, Springfield, Virginia (1968).
44. S. K. Kao. "A Model for Turbulent Diffusion over Terrain." *J. Atmos. Sci.* 33, 157 (1976).
45. M. E. Smith. *Recommended Guide for the Prediction of the Dispersion of Airborne Efficients*. ASME (1973).

NOMENCLATURE

α_1 = error variance in horizontal velocity	K_z = vertical diffusion (turbulence)
α_2 = error variance in vertical velocity	L = Obukhov atmospheric stability length
C = concentration g/m^3	$\{\lambda\}$ = column matrix of unknown values of Lagrangian multipliers
C_0 = mean concentration	λ = Lagrangian multiplier
C_i = zeroth moment (concentration) within cell i	$[M]$ = sparse coefficient matrix containing 7 diagonals
C_0' = mean concentration just outside of sol'n domain	N = partial differential equations
ϵ = turbulent eddy dissipation rate	\hat{n}_h = unit vector normal to surface
F_i = first moment (concentration) within cell i	\hat{n}_H = outwardly directed unit vector normal to surface
f_0 = mass flux of concentration at surface	v_g = actual settling velocity
η = lateral direction	ξ = longitudinal direction
θ^* = temperature friction values at the surface	P_i = portioning parameter
$h(x,y)$ = ground elevation at (x,y)	p = deposition velocity
H = elevation of upper limit for vertical mixing	$\{q\}$ = column matrix of explicitly known values
\tilde{H} = height of release	Q = continuous emission rates
κ = von Karman's constant	ρ = vertical direction
\hat{K} = directionally dependent eddy diffusivity exchange coefficient of diffusion	r = reflection coefficient
K_m = exchange coefficient of momentum	R_i = second moment (concentration) within cell i
K_t = exchange coefficient of heat	S = source and sink terms associated with precipitation, deposition, etc.
K_x = horizontal (longitudinal) diffusion	σ_a = standard deviation of the azimuthal wind fluctuation
K_y = lateral diffusion	γ = Courant number
	Δt = time step
	τ = nondimensional time

- U^* = velocity friction values at the surface
 \vec{U} = vector velocity field
 ϕ_m = nondimensional velocity gradient
 ϕ_t = nondimensional temperature gradient
 \tilde{W} = transformed vertical velocity
 δ_i = relative displacement of material within the i^{th} cell from the center of the cell
- $x_w, x_e, y_r, y_s = W, E, N, S$ lateral boundaries within the x, y plane

Subscripts

- m = momentum
 t = temperature
 i = cell location
 a = azimuth
 H = mixing height
 i, j, k = finite difference grid at point ξ, η, ρ

Superscripts

- $*$, $**$, $***$ = intermediate concentration values between n and $n+1$ time step
 \sim = normalized value

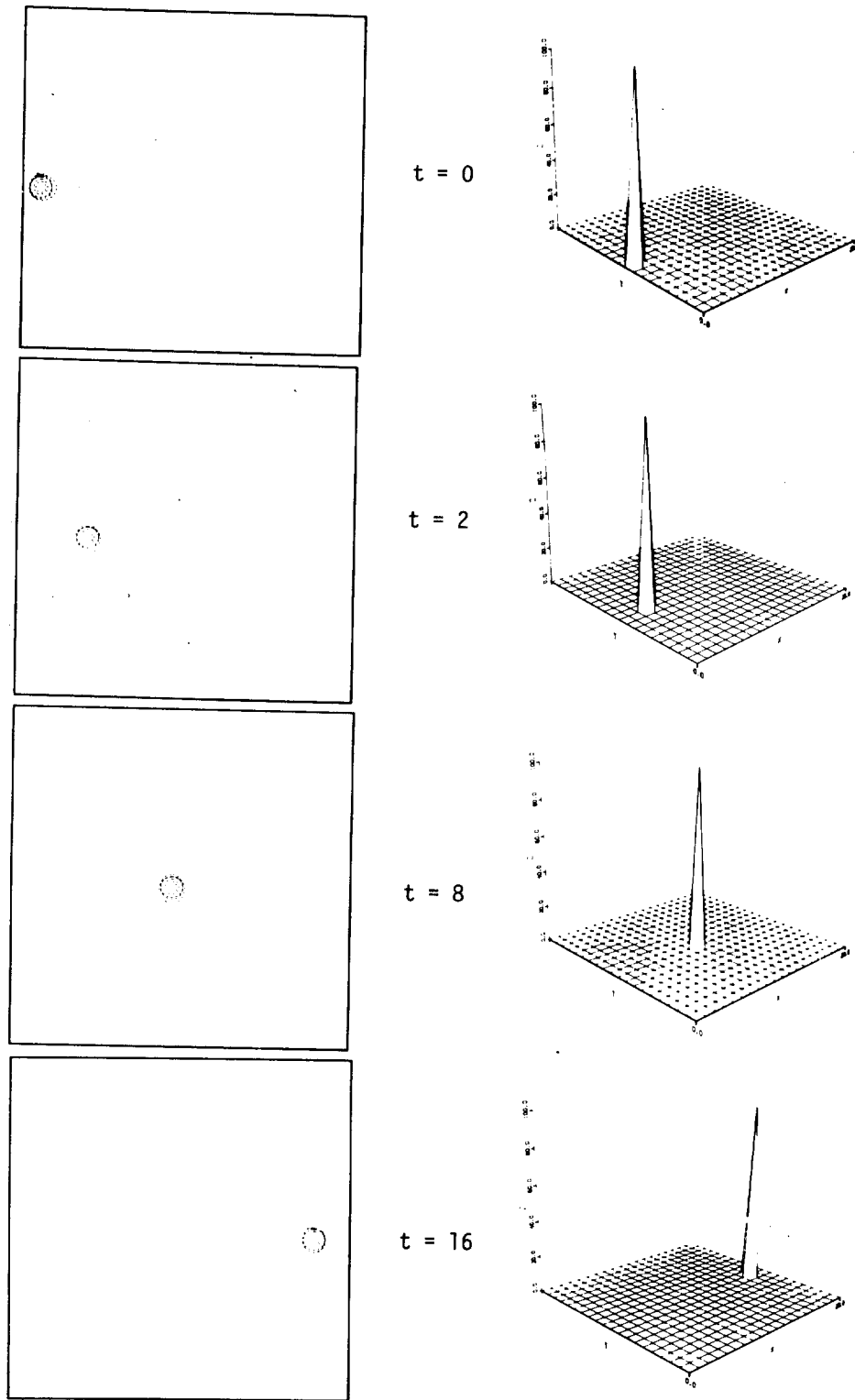


FIGURE 1. Advection of a Cell of Concentration ($C = 100$) in One Dimension; $\vec{U} = (1,0,0)$; $\Delta X = \Delta Y = 1$; $\Delta t = 0.5$

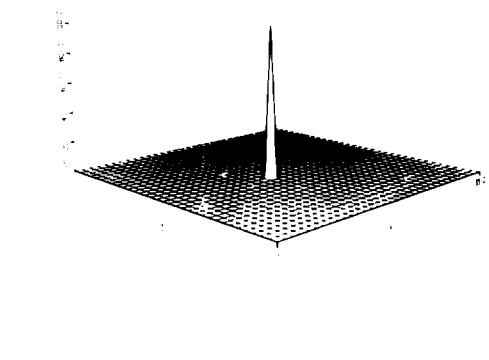
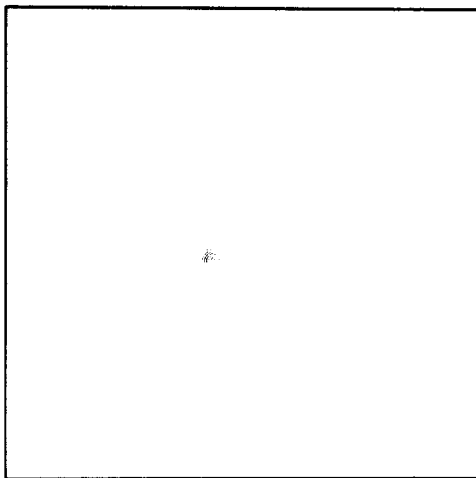
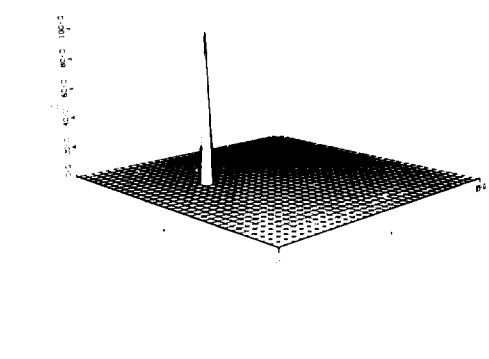
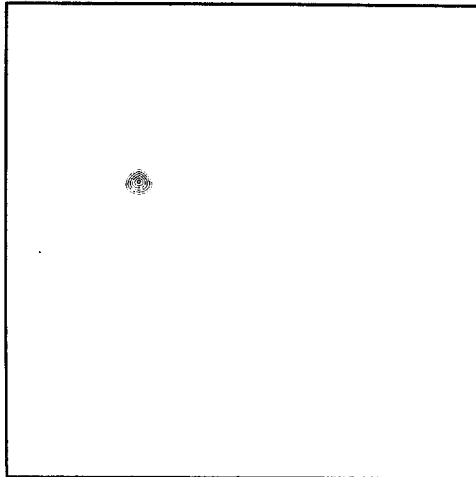
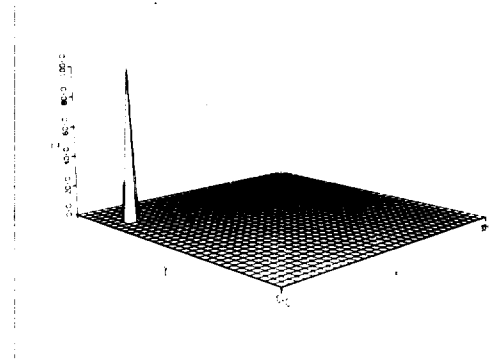
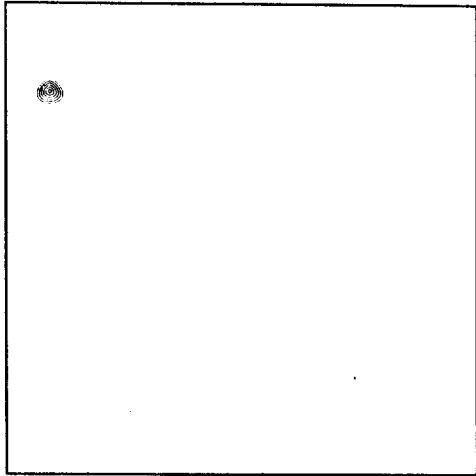
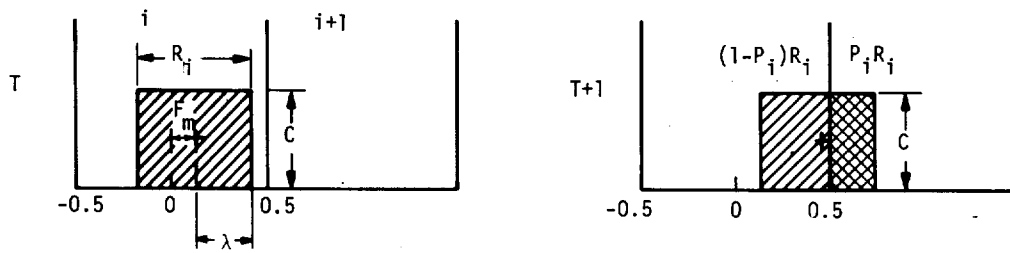
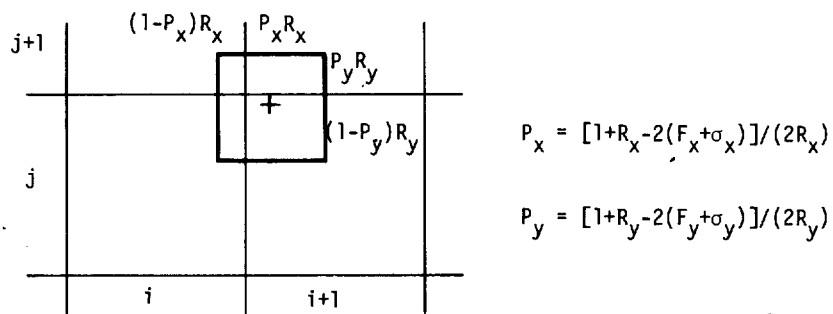


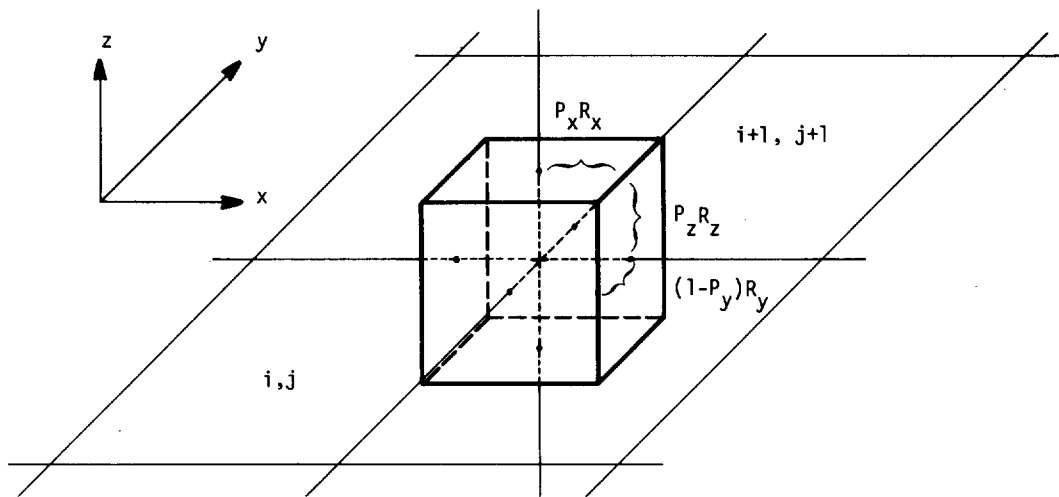
FIGURE 2. Advection of Concentration ($C = 100$) in Two Dimensions;
 $V = (1,1,0)$; $\Delta X = \Delta Y = 1$; $\Delta t = 0.5$



a) One Dimensional Advection



b) Two Dimensional Advection



c) Three Dimensional Advection

FIGURE 3. Scaling Parameters Used in Advection of Cell of Concentration

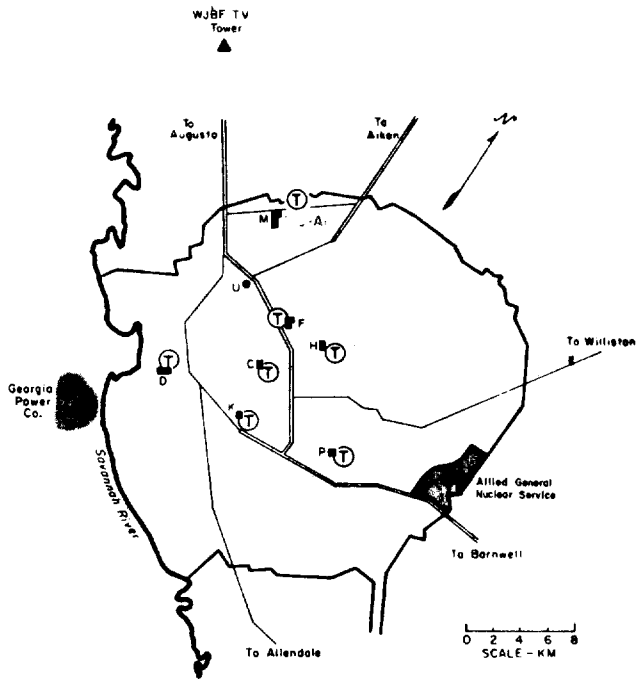
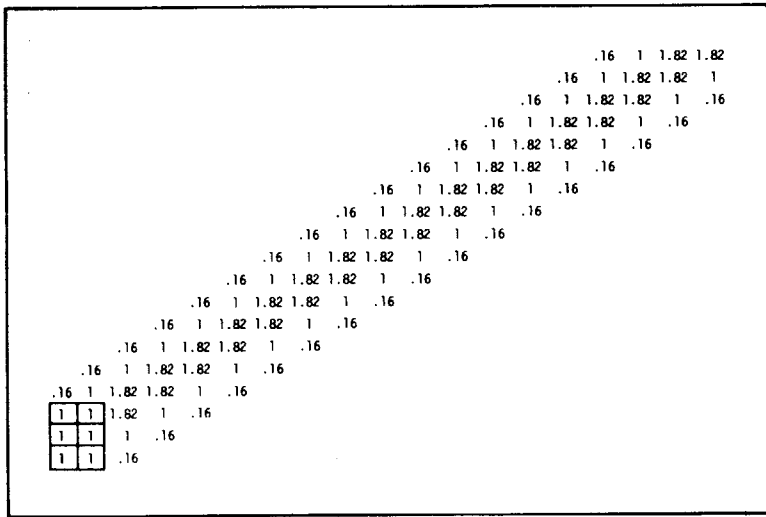
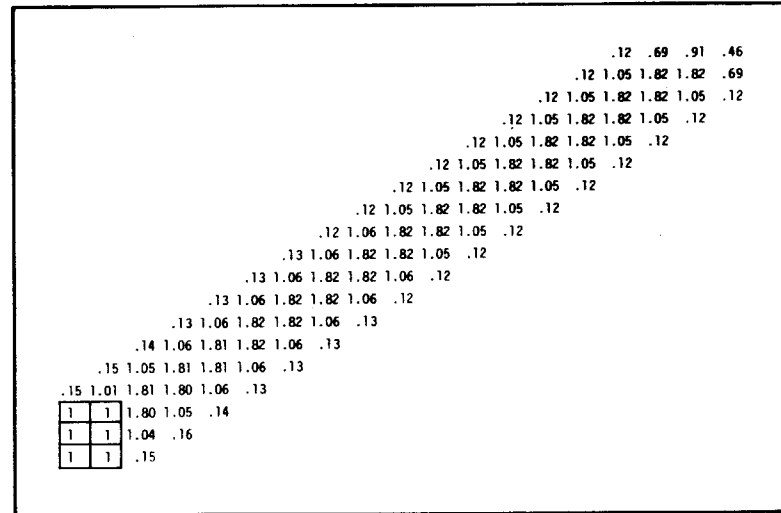


FIGURE 4. Location of the Severe Meteorological Towers within SRP and the WJBF-TV Tower



Analytical Solution (Pedersen & Prahm, 1974)



Numerical Solution

FIGURE 5. Advection of Concentration from a Continuous Area Source ($Q = 1/\text{cell}$); $U = (1,1,0)$; $\Delta X = \Delta Y = 1$, $\Delta t = 0.5$

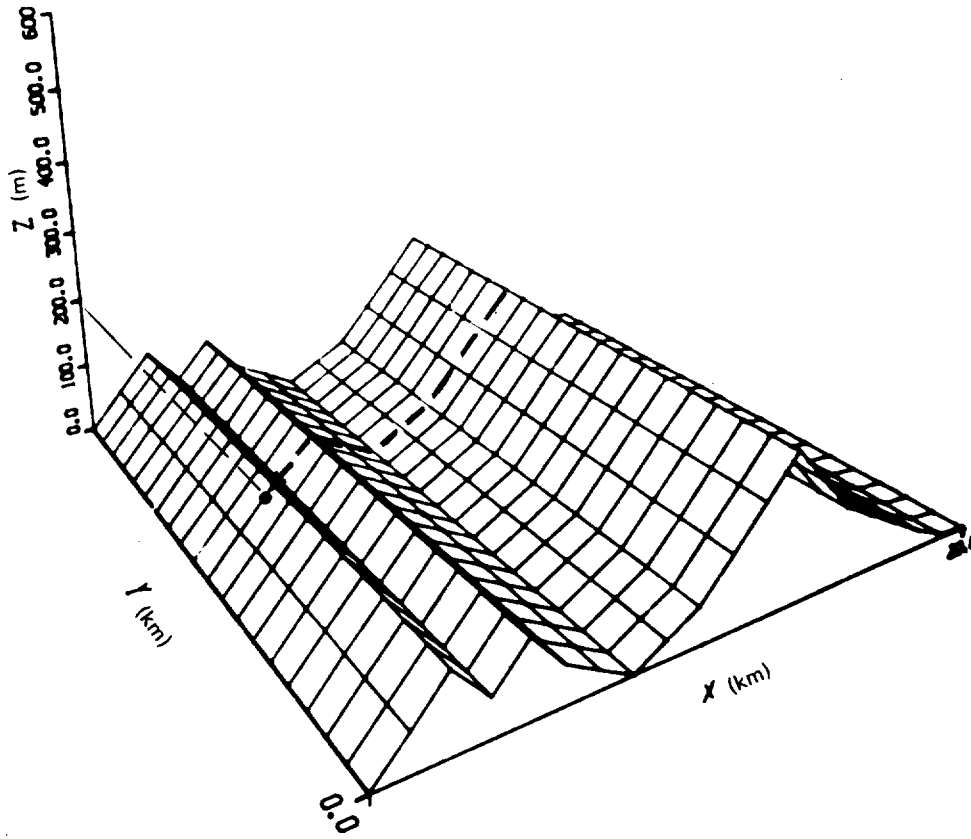
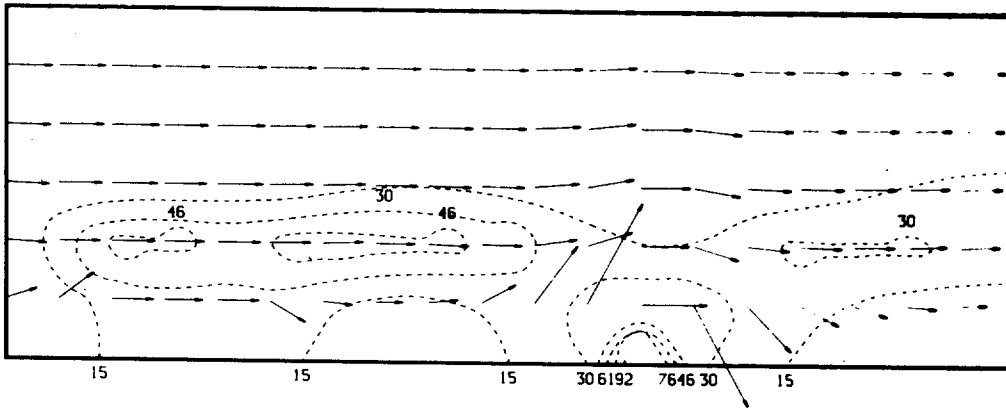
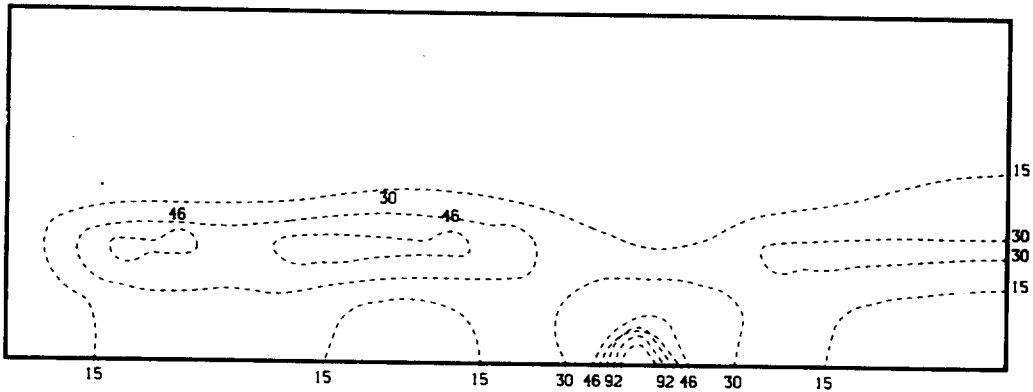


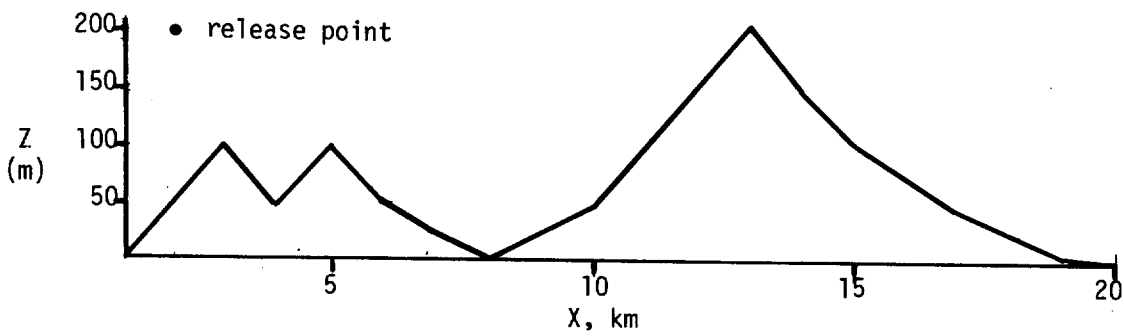
FIGURE 7. Topographic Surface for Continuous Elevated Emissions Prediction



a.) Concentration isopleths at $t = 1$ hour; wind vectors drawn for steady state velocities (vertical velocity component increased to enhance visualization)



b.) Concentration isopleths at $t = 4$ hours (\sim steady state)



c.) Topography in the $x-z$ plane at $y = \frac{1}{2}$

FIGURE 8. Concentration Isopleths in the $\xi-\rho$ Plane at $\eta = 1/2$

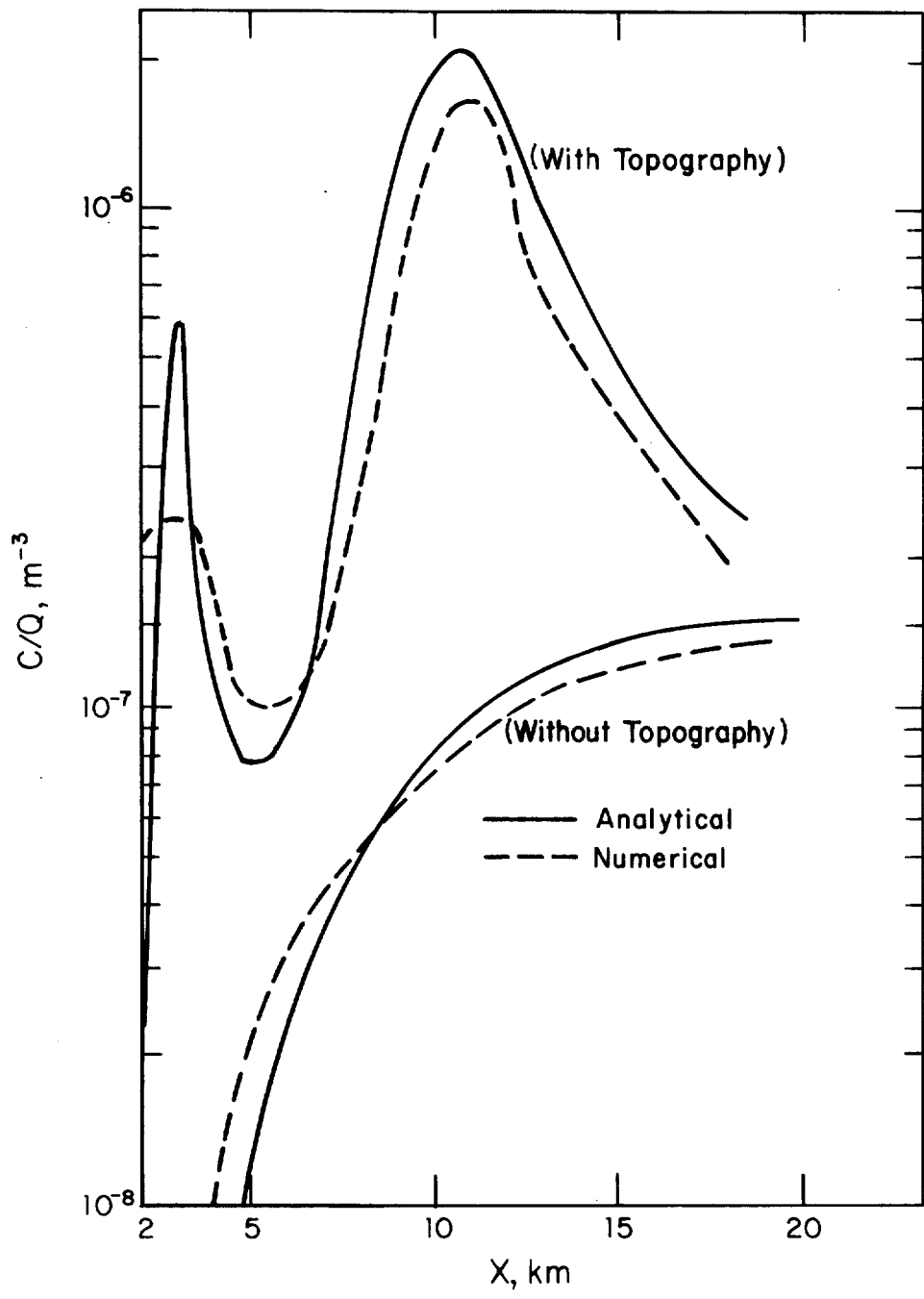


FIGURE 9. Ground Level Centerline C/Q Values

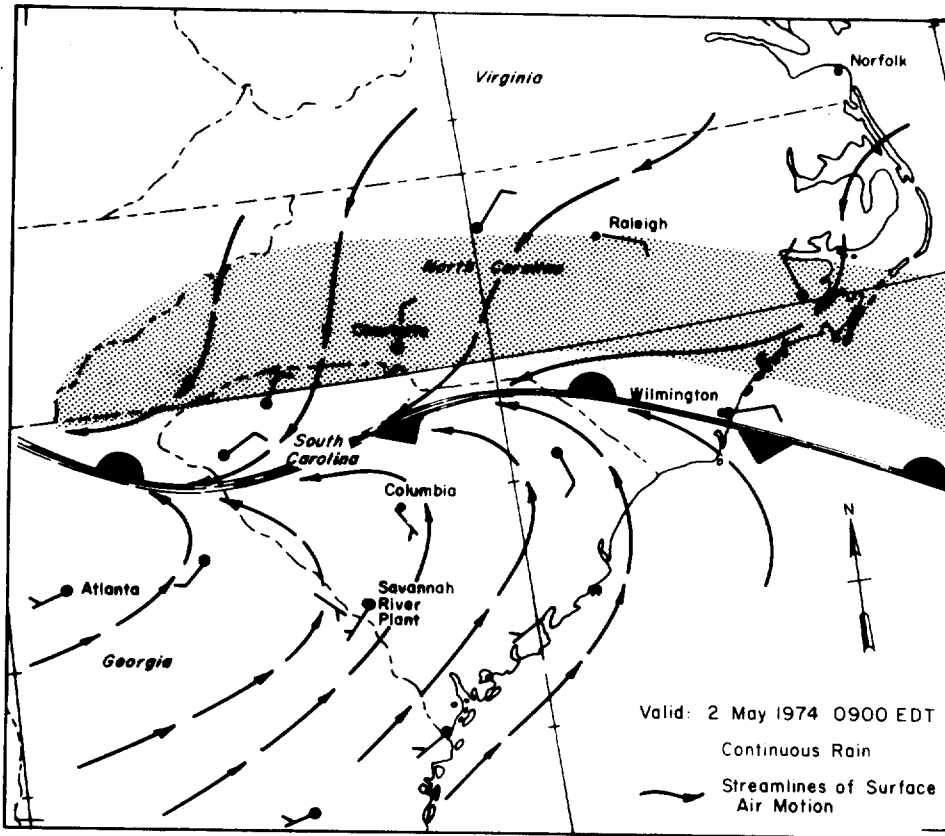


FIGURE 10. Synoptic Wind Field for the Southeast on May 2, 1974

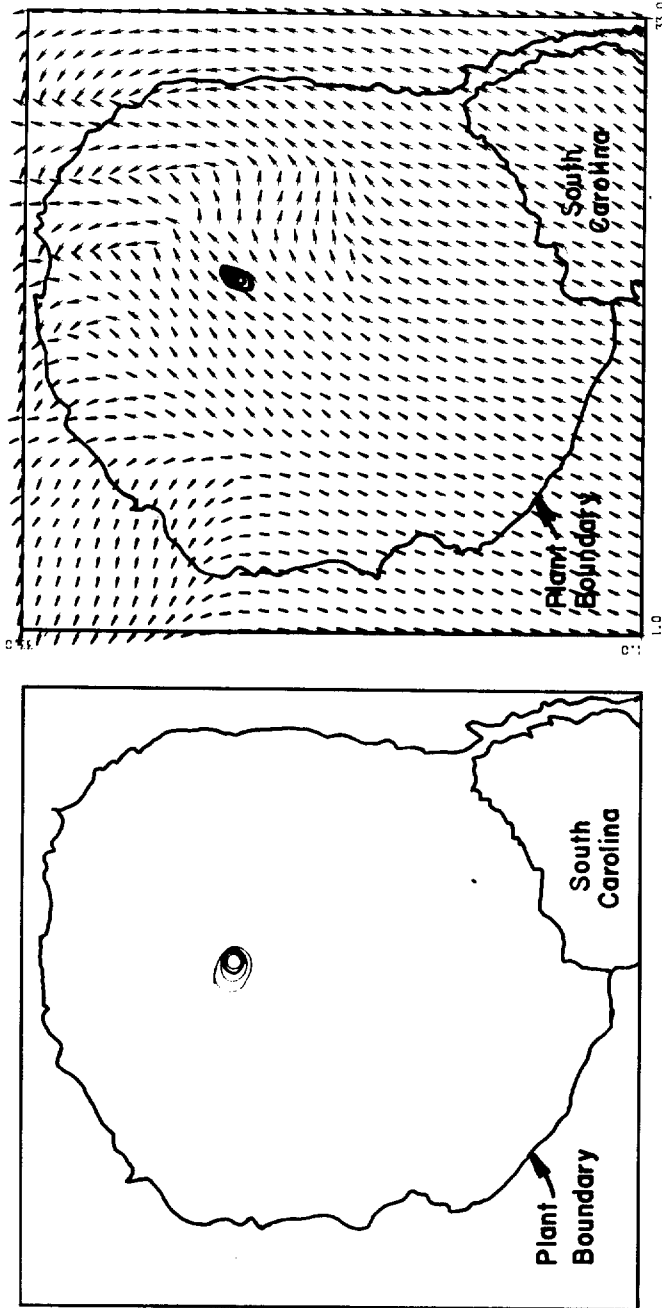


FIGURE 11. Initial Concentration Distribution and Wind Field for May 2, 1974 Tritium Release

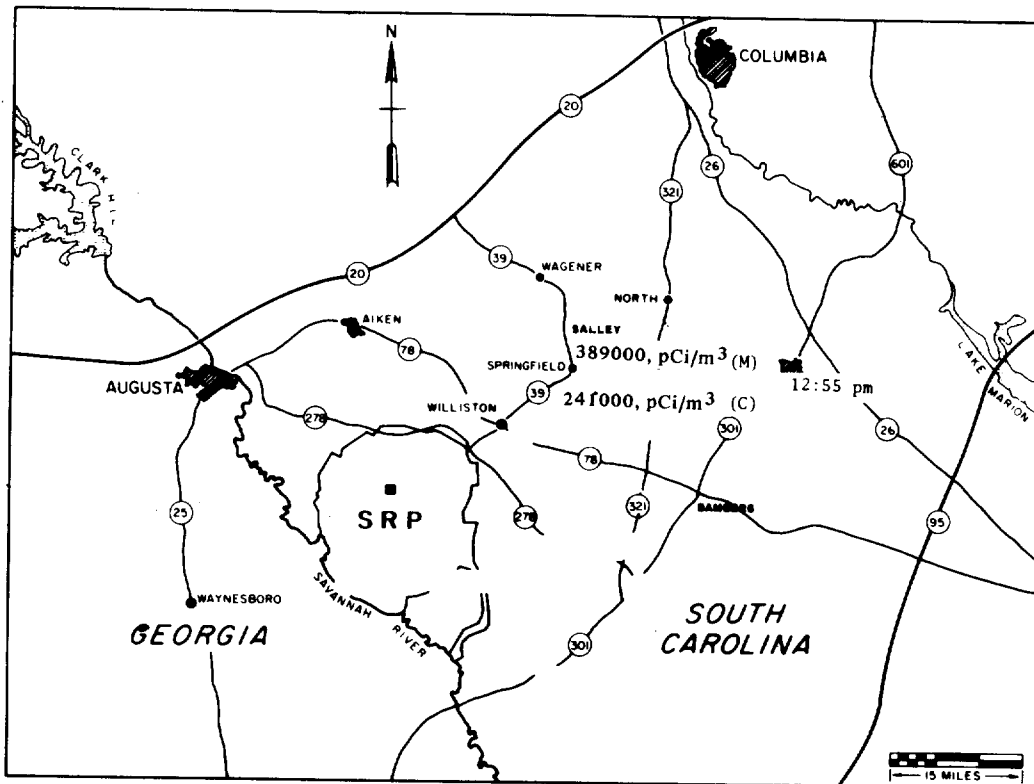


FIGURE 12. Numerical Result at Ground Level at Springfield, South Carolina for the May 2, 1974, Tritium Release. Initial release time was approximately 0800 EDT. M = measured value; C = calculated value.